A novel genetic marginalized particle filter method for state of charge and state of energy estimation adaptive to multi-temperature conditions of lithium-ion batteries.

JIA, X., WANG, S., CAO, J., QIAO, J., YANG, X., LI, Y. and FERNANDEZ, C.

2023

A novel genetic marginalized particle filter method for state of charge and state of energy estimation adaptive to multi-temperature conditions of lithium-ion batteries

Xianyi Jia [a,c], Shunli Wang [a,b,*], Wen Cao [a], Jialu Qiao [a], Xiao Yang [a], Yang Li [a], Carlos Fernandez [d]

[a] School of Information Engineering, Southwest University of Science and Technology, Mianyang 621010, China
[b] College of Electrical Engineering, Sichuan University, Chengdu 610065, China
[c] Tsinghua Sichuan Energy Internet Research Institute, Chengdu 610299, China
[d] School of Pharmacy and Life Sciences, Robert Gordon University, Aberdeen AB10-7GJ, UK
* Corresponding author: Shunli Wang Email address: 497420789@qq.com

A B S T R A C T

Power lithium-ion batteries are widely used in various fields, the battery management system (BMS) is the main object of battery energy management and safety monitoring, so the accurate collaboration of state of charge (SoC) and state of energy (SoE) is estimated to be essential for the BMS system. In this work, a novel genetic marginal particle filter (GMPF) algorithm to estimate SoC and SoE accurately. The forgetting factor recursive least square (FFRLS) algorithm is used to identify the second-order Thevenin equivalent model parameter, and the genetic algorithm is used to improve the re-sampling process of the traditional particle filtering (PF) algorithm, according to the Rao-Blackwell theory in statistical science, the marginalization of part of the linear state variables during the calculation of particle filtering, the distribution of the post-test is similar to a single Gaussian distribution. The GMPF algorithm is verified under the conditions of the hybrid pulse power characteristic (HPPC) and the Beijing bus dynamic stress test (BBDST) with 15 °C, 25 °C, and 35 °C respectively, and experimental results show that the improved GMPF algorithm can effectively realize the collaborative estimation of the SoC and SoE of power lithium-ion batteries. The mean absolute error of SoC and SoE estimation is always less than 1.56 %, the root-mean-square error is always less than 1.58 %. And the GMPF algorithm is suitable for temperature environments of 15 °C to 35 °C.

Keywords:
State of charge; State of energy; Genetic marginalized particle filter; Multi-temperature; Battery management system; Lithium-ion battery

1. Introduction

With the development of society, the energy demand has continued to increase, energy is continuously enriched by consumption scenes, and the demand for energy storage in the world has become stronger [1]. Lithium-ion batteries have become the main components of the application of energy storage systems with their long life, high stability, high energy density, and moderate advantages [2]. Lithium-ion battery types are divided into power batteries, energy storage batteries, and consumer batteries. Power lithium-ion batteries usually refer to lithium-ion batteries that provide power sources for high-power devices [3]. They have the characteristics of large energy density, small volume, and high single voltage. Therefore, power lithium-ion batteries are not only used in the field of new energy vehicles but also the fields of robots and drones [4].

Compared with the use of traditional energy, drones and robots with power lithium-ion batteries as power sources have the characteristics of lightness and flexibility [5].

Currently, commonly used cathode materials for lithium-ion batteries in the market include lithium cobalt oxide, lithium iron phosphate, and ternary compounds [6]. Among them, the structure of lithium cobalt oxide batteries is unstable, so lithium iron phosphate and ternary lithium batteries are the most widely used in the market [7]. As the battery market continues to expand, more and more energy storage fields are starting to use ternary lithium-ion batteries with higher energy density for better product performance and user experience. Ternary lithium-ion batteries with high energy density advantages and fast charging efficiency have great potential for large-scale market applications in some consumer electronics products that value user experience [8]. However, the unstable chemical characteristics of ternary lithium- ion batteries have limited their development [9]. The key to breaking through the existing situation of new energy is whether the battery's safety performance can be ensured by real-time monitoring of the battery's state at the battery management level.

For battery pack systems with high integration and high energy density, ensuring their safety and reliability during power output and energy storage processes, as well as real-time monitoring, is crucial. Therefore, the Battery Management System (BMS) for lithium-ion batteries, which is responsible for battery energy management and safety monitoring, has become an indispensable core for the use of lithium-ion batteries as a source of energy and power [10]. A high-performance BMS can not only accurately measure key reference information such as battery voltage, current, and temperature, but also perform system safety diagnosis and danger alarms, as well as accurately estimate the state of charge (SoC) and state of energy (SoE) [11]. It can combine actual conditions to manage battery energy consumption and improve battery energy utilization efficiency. Since parameters such as SoC and SoE are hidden and cannot be directly measured, and the estimation results are easily affected by noise, significant estimation errors may occur [12]. Therefore, accurately and efficiently estimating the state parameters of the battery has become a major research focus in today's battery management systems.

SoC is an intuitive display of the remaining capacity of a lithium-ion battery. Generally speaking, it is defined as the ratio of the amount of electricity that can be discharged from the current state of the battery to the rated capacity [13]. Accurate and reliable SoC is the foundation for ensuring normal user use and can optimize the charging and discharging strategies of lithium-ion batteries [14]. SoC can provide effective reference for the state of the battery, provide data and correction plans for energy management of power lithium-ion batteries, and is the cornerstone of BMS for predictive analysis [15]. Accurately estimating the SoC value is crucial to ensuring the performance of battery packs, improving cycle life, and reducing usage costs. As a typical secondary battery, the essence of the charge and discharge of lithium-ion batteries is

the intercalation and deintercalation of lithium-ions between the positive and negative electrodes [16]. At the same time, a series of side reactions occur between the positive and negative electrodes and the electrolyte, which means that there are multiple interrelated electro-chemical reactions inside the battery [17]. However, in practical applications, the complexity and diversity of the battery's working environment, as well as issues such as aging due to frequent use, over-charging, and over-discharging, all affect the internal reaction process of the lithium-ion battery, greatly increasing the difficulty of estimating the battery's SoC [18]. Therefore, an accurate and reliable SoC estima-tion strategy has become one of the urgent problems that BMS needs to solve.

SoE refers to the changes in the energy status of a battery, which takes into account the variations in the battery voltage on the basis of SoC. Although the estimation of SoE is more challenging, it has greater advantages over SoC when used for estimating the remaining discharge time and energy of a subsequent power lithium-ion battery [19]. As the future prospects for the application of power lithium-ion batteries in various industries are vast, BMS systems require higher accuracy and stability [20]. Therefore, strengthening the research on the algorithm for estimating the SoE of lithium-ion batteries is of significant importance [21]. At present, in the use of power lithium-ion batteries, SoE is an important basis for estimating the remaining usage time or mileage [22]. If the estimated SoE result is greater than the actual result, it can lead to over-discharge of the power lithium-ion battery, which h can cause irreversible damage to the battery itself, not only reducing its lifespan but also posing significant safety issues [23]. If the estimated SoE value is smaller than the actual value, it will lead to reduced usage efficiency, which cannot effectively utilize the efficiency of the power lithium-ion battery [24]. Therefore, in order to effectively solve safety and efficiency issues, and extend the lifespan of power lithium-ion batteries, accurate SoE estimation is also one of the urgent problems that BMS needs to solve [25].

Currently, lithium-ion battery SoC and SoE estimation algorithms mainly include direct measurement methods, model-based estimation methods, neural network-based estimation methods, and hybrid methods [26]. For example, although direct measurement methods have high estimation accuracy, they require very accurate SoC-OCV and SoE- OCV correspondence and also have high requirements for measuring instruments [27]. methods are easy to operate and have high accuracy, but they require a large number of training samples to ensure measurement accuracy and are therefore not suitable for small sample sizes [28]. Model-based estimation methods ensure accuracy by constructing an accurate equivalent model, and they and the hybrid methods that include them are currently the most widely used methods [6]. Under these methods, the estimation effect mainly needs to consider convergence, accuracy, and universality.

Fan et al. [29] proposed a novel long short-term memory network combined with an adaptive unscented Kalman filter (LSTM-AUKF) method to estimate SoC and SoE simultaneously, and its accuracy has been verified under different operating conditions. Wang et al. [30] estimated SoC and SoE using different models and methods respectively, and verified their accuracy under different operating currents. A combined SoC and SoE estimation using the dual forgetting factor adaptive extended Kalman filter (DFFAEKF) algorithm and experimental quantitative relations between SoC and SoE are utilized to estimate the SoC and SoE by Shrivastava et al. [25]. Zhang et al. [31] taking identified open-circuit voltage as observation information, two first-order EKFs are established to online estimate SoC and SoE. Ma et al. [32] investigated a novel data-driven method that can estimate SoC and SoE simultaneously based on a long short-term memory (LSTM) deep neural network. Wei et al. [33] proposed a method for estimating the SoE of lithium-ion batteries using the Unscented Particle Filter (UPF).

With the goal of achieving high-precision simultaneous estimation of SoC and SoE for ternary lithium-ion batteries, this paper considers aspects such as estimation convergence, accuracy, and universality. Rather than using the coupling relationship between SoC and SoE for joint estimation, the paper separately estimates SoC and SoE at the same time scale to improve estimation accuracy. A second-order Thevenin equivalent circuit model is established, taking into account the accurate characterization of battery polarization effects and computational complexity. The FFRLS algorithm is used for parameter identification of the model to solve the problem of untimely data processing and inability to update parameters in real-time caused by offline parameter identification. To address the issue of particle impoverishment in traditional particle filtering algorithms, a genetic algorithm is used to improve the resampling process of traditional particle filtering, reducing conver-gence time and improving convergence. Additionally, Rao-Blackwell theory in statistics is used to marginalize some of the linear state vari-ables in the calculation process of particle filtering, reducing estimation variance and improving estimation accuracy. Finally, the proposed method is validated under multiple temperatures and operating conditions. Experimental results show that the proposed GMPF algorithm can effectively achieve cooperative estimation of SoC and SoE for dynamic lithium-ion batteries. Moreover, the MAE of SoC estimation under HPPC and BBDST operating conditions can be maintained within 1.56 %, with RMSE maintained within 1.25 % under multiple temperature condi-tions. The MAE of SoE estimation can be maintained within 1.56 %, with RMSE maintained within 1.58 %. These results demonstrate the universality of the proposed method.

The problems that the proposed method in this paper can solve are as follows: First, estimating SoC and SoE for ternary lithium-ion batteries separately at the same time scale avoids the problem of one estimation error leading to a larger estimation error for the other due to the interrelationship between the two. Second, the proposed GMPF algorithm solves the problem of particle impoverishment in traditional particle filtering, improving the estimation accuracy of SoC and SoE for lithium-ion batteries. Third, the proposed GMPF algorithm improves the convergence of the estimation of SoC and SoE for lithium-ion batteries and can converge at the initial moment of operation. Fourth, the proposed method is validated under multiple temperatures and operating conditions, demonstrating the effectiveness and good universality of the proposed method.

The rest of this paper is organized as follows: Section 2 is the theoretical analysis part of this paper. Section 2.1 establishes the model for the lithium-ion battery and relevant calculations, while Section 2.2 provides a detailed introduction and calculation of the online parameter identification algorithm based on the forgetting factor. Section 2.3 provides a detailed introduction of the proposed GMPF algorithm and its improvements. Section 3 is the experimental verification part of this paper. Section 3.1 validates the online parameter identification results, while Section 3.2 verifies the proposed method under the HPPC operating condition with multiple temperature conditions. Section 3.3 verifies the proposed method under the BBDST operating condition with multiple temperature conditions. Section 4 is the conclusion and outlook of this paper.

2. Mathematical analysis

2.1. Equivalent circuit modeling

Unlike the electrochemical model, most equivalent circuit model structures are relatively simple, they have few parameters and are easy to recognize. It consists of components such as voltage sources, resistors, and capacitors, current and voltage data can be obtained by charging and discharge experiments, and then we can use the parameter recognition method to obtain model parameters. The equivalent model is built based on experience, the chemical reactions inside the battery are not studied, because of low calculation complexity, they are widely used in battery status estimation.

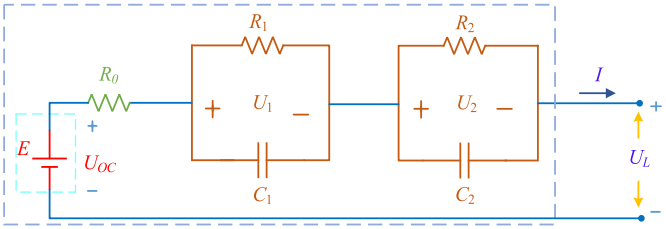

Fig. 2-1. Second-order Thevenin model.

Whether SoC is accurately estimated to a large extent depends on the accuracy and complexity of the model, under the premise of accurately indicating the dynamic performance of the battery, a model with a suitable complexity should be selected. The Thevenin model and the PNGV model are not enough to accurately simulate the battery polarization effect, if here are many RC circuits, computing will be more complicated. Therefore, this article selects the second-order Thevenin model from the equivalent circuit models, which can accurately simulate the battery polarization effect, the model is simpler and suit-able for engineering. The Thevenin model as shown in Fig. 2-1.

According to the law of Kirchhoff, the state-space equation can be obtained, as shown in Eq. (2-1):

$$\begin{cases} U_L = U_{oc}(SoC/SoE) - IR_0 - U_1 - U_2 \\ \dfrac{dU_1}{dt} = -\dfrac{U_1}{R_1C_1} + \dfrac{I}{C_1} \\ \dfrac{dU_2}{dt} = -\dfrac{U_2}{R_2C_2} + \dfrac{I}{C_2} \end{cases} \tag{2-1}$$

In the Eq. (2-1), U_{oc} represents the opening voltage, U_L is the end voltage of the lithium-ion battery, R_0 is the ohmic resistance; R_1 and C_1 are electrochemical polarization internal resistance and polarization capacitors, respectively; R_2 and C_2 are thick polarization resistors and polarization capacitors, respectively; I is a dry road current, U_1 and U_2 are voltages of parallel networks of R_1C_1 and R_2C_2, respectively. The SoC definition as shown in Eq. (2-2).

$$SoC_t = SoC_{t_0} - \frac{\eta_1}{C_n}\int_{t_0}^{t} I_{(t)}dt \tag{2-2}$$

In the Eq. (2-2), SoC_t is the SoC value of time t, C_n is the rated capacity of the battery, η_1 is the charge and discharge efficiency. $[SoC\ U_1\ U_2]$ is the state variable at the input terminal in the second-order Thevenin model, the SoC's discrete state spatial equation is like Eq. (2-3).

$$\begin{cases} \begin{bmatrix} SoC(k+1) \\ U_1(k+1) \\ U_2(k+2) \end{bmatrix} = \begin{bmatrix} 1 & 0 & 0 \\ 0 & e^{-\frac{1}{R_1C_1}} & 0 \\ 0 & 0 & e^{-\frac{1}{R_2C_2}} \end{bmatrix} \begin{bmatrix} SoC(k) \\ U_1(k) \\ U_2(k) \end{bmatrix} + \begin{bmatrix} -\dfrac{\eta_1}{C_n} \\ R_1\left(1-e^{-\frac{1}{R_1C_1}}\right) \\ R_2\left(1-e^{-\frac{1}{R_2C_2}}\right) \end{bmatrix} I_k + \begin{bmatrix} \omega_1(k+1) \\ \omega_2(k+1) \\ \omega_3(k+1) \end{bmatrix} \\ U_t(k+1) = U_{oc}(k+1) - U_1(k+1) - U_2(k+1) - R_0I_k + v(k+1) \end{cases} \tag{2-3}$$

In the Eq. (2-3), $\omega_i(i=1,2,3)$ is process noise, v is the measuring noise, U_{OC}, R_2, R_0, R_1, C_1, and C_2 are parameters need to be identified in the model. The power integrator method is similar to amp-hour integrator in the process of SoC estimation, it is based on the battery SoE definition method to integrate the power, the value of energy changed can be got from the integral of battery current and voltage, then the current SoE value of the battery can be obtained. The SoE's calculation expression as shown in Eq. (2-4).

$$SoE = SoE_0 - \frac{\int_0^t \eta IUdt}{3600E_N} \tag{2-4}$$

In the Eq. (2-4), SoE_0 is the initial value of battery SoE, η is the charge and discharge efficiency of the battery. I is a battery load current, the discharge direction is positive, the unit is A, U is the battery side voltage, the unit is V. T is working time, the unit is s, E_N is the rated energy of the battery, and the unit is Wh. SoE discrete expression as shown in Eq. (2- 5).

$$SoE_{k+1} = SoE_k - \frac{\eta_k\Delta E_k}{E_N} = SoE_k - \frac{\eta_k I_k U_{L,k}\Delta t}{E_N} \tag{2-5}$$

In the Eq. (2-5), ΔE_k is the consumed energy at time of k, I is the load current of the battery at the time of k, $U_{L,k}$ is the terminal voltage of the lithium-ion battery at time of k, Δt is the sampling interval.

2.2. Forgetting factor recursive least square algorithm

In the study of battery SoC and SoE estimation, the method of offline experimental data fitting function is generally used to determine the value of each parameter in the battery model. But this way will cause a large error in the estimation results, and the parameter value obtained from offline recognition is fixed, it does not reflect the actual situation of model parameters at each moment. In order to improve the accuracy of parameter identification, fully express the actual changes of each parameter in the using of lithium-ion batteries. Therefore, the online recognition of the model parameter and the real-time correction of the parameters are particularly important.

The ordinary minimum daily method has a large matrix calculation, and the disadvantages such as online recognition cannot be performed. In order to solve these problems, recursive least square (RLS) can be used, it can get a gain coefficient form based the collaborative differential matrix, it can modify the parameter estimation value of each time, in the process of pushing every time, you can get accurate parameter estimation results. However, the phenomenon of "data saturation" is prone to occur during the recursive process, in other words, the trust of RLS allocated to at any moment is the same, which will lead to more and more old data accumulation, The information of the old data has been obtained at the previous moment. The information of the new data is covered by the old data. The information obtained from the new data is reduced. The correction ability of the algorithm will gradually weaken.

In order to avoid the phenomenon of "data saturation", it is necessary to distribute more trust to the newly collected data, to maximize the weight of the old data occupied. Therefore, the forgotten factor is added to the RLS algorithm, this way will improve the online estimate of the RLS algorithm. Forgotten factor can distribute greater weights to new data, it can strengthen the feedback effect of new data in parameter recognition, and gradually reduce the impact of the old data, therefore, the information provided by the new data will not be covered by old data, it can strengthen the correction ability of the algorithm so that the algorithm can always achieve a fast convergence. The improved target function is shown in Eq. (2-6).

$$J = \sum_{k=n+1}^{N} \lambda^{N-k} [e(k)]^2 \tag{2-6}$$

In the Eq. (2-6), λ is forgotten factor, and its value range is 0 to 1, different values will have different accuracy, $e(k)$ is an error collaboration matrix, the Gaussian white noise sequence is applied to it. Then the recursive Equation of the FFRLS algorithm is shown in Eq. (2-7).

$$\begin{cases} \widehat{\theta}(k+1) = \widehat{\theta}(k) + K(k+1)\left[y(k+1) - \phi^T(k+1)\widehat{\theta}(k)\right] \\ K(k+1) = P(k+1)\phi(k+1)\left[\phi^T(k+1)P(k)\phi(k+1) + \lambda\right]^{-1} \\ P(k+1) = \lambda^{-1}\left[I - K(k+1)\phi^T(k+1)\right]P(k) \end{cases} \tag{2-7}$$

In the Eq. (2-7), λ is closer to 1, the simulation results will be better, the value of λ is 0.98 in this simulation. The smaller the λ, the faster the algorithm, but it will also cause the fluctuation of the algorithm. When $\lambda = 1$, it is standard recursive least square algorithm. Then the battery model is converted into minimum daily mathematical forms, as shown Eq. (2-8).

$$U_{OC} - U_L = \left(R_0 + \frac{R_1}{1+\tau_1 s} + \frac{R_2}{1+\tau_2 s}\right) I \tag{2-8}$$

In the Eq. (2-8), The FFRLS algorithm is used in the equivalent model parameter recognition of the lithium-ion battery, in this way, the parameters in the second-order Thevenin equivalent circuit model are identified. Time constant $\tau_1 = R_1C_1$, $\tau_2 = R_2C_2$, then Eq. (2-8) can be rewritten to Eq. (2-9).

$$\begin{aligned} &\tau_1\tau_2 U_{OC}s^2 + (\tau_1+\tau_2)U_{OC}s + U_{OC} = \tau_1\tau_2 R_0 {I_s}^2 + [R_1\tau_2 + R_2\tau_1 + R_0(\tau_1+\tau_2)]I_s \\ &+(R_1+R_2+R_0)I + \tau_1\tau_2 U_{Ls}^2 + (\tau_1+\tau_2)U_{Ls} + U_L \end{aligned} \tag{2-9}$$

In the Eq. (2-9), U_{oc} represents battery opening voltage, R_0 represents ohmic resistance of the battery. Supposing $a = \tau_1\tau_2$, $b = \tau_1 + \tau_2$, $c = R_1 + R_2 + R_0$, $d = R_1\tau_2 + R_2\tau_1 + R_i(\tau_1+\tau_2)$, then the Eq. (2-9) can be simplified to Eq. (2-10).

$$aU_{OC}s^2 + bU_{OC}s + U_{OC} = aR_0{I_s}^2 + dI_s + cI + aU_{Ls}^2 + bU_{Ls} + U_L \quad s = [x(k) - x(k-1)]/T \quad \text{and} \quad s^2 = [x(k) - 2x(k-1) + x(k-2)]/T^2 \tag{2-10}$$

were brought into Eq. (2-10) for discrete treatment, T is the sampling time, then the Eq. (2-10) can be written into Eq. (2-11).

$$\begin{aligned} &U_{OC}(k) - U_L(k) = \frac{-bT - 2a}{T^2 + bT + a}[U_L(k-1) - U_{OC}(k-1)] + \\ &\frac{a}{T^2 + bT + a}[U_L(k-2) - U_{OC}(k-2)] + \frac{cT^2 + dT + aR_0}{T^2 + bT + a}I(k) + \\ &\frac{-dT - 2aR_0}{T^2 + bT + a}I(k-1) + \frac{aR_0}{T^2 + bT + a}I(k-2) \end{aligned} \tag{2-11}$$

Ordering $k_1 = \frac{-bT-2a}{T^2+bT+a}$, $k_2 = \frac{a}{T^2+bT+a}$, $k_3 = \frac{cT^2+dT+aR_i}{T^2+bT+a}$, $k_4 = \frac{-dT-2aR_i}{T^2+bT+a}$, $k_5 = \frac{aR_i}{T^2+bT+a}$, and $\theta = [\,k_1\,k_2\,k_3\,k_4\,k_5\,]$ is used as a direct recognition parameter, realizing the results of these parameters to derive the circuit model parameters, then ordering $k_0 = T^2 + bT + a$, Eq. (2-12) can be showed:

$$\begin{cases} k_0 = \dfrac{T^2}{k_1 + k_2 + 1} \\ a = k_0 k_2 \\ b = \dfrac{-k_0(k_1 + 2k_2)}{T} \\ c = \dfrac{k_0(k_3 + k_4 + k_5)}{T^2} \\ d = \dfrac{-k_0(k_4 + k_5)}{T} \\ R_0 = \dfrac{k_5}{k_2} \end{cases} \tag{2-12}$$

In the Eq. (2-12), the value of R_0 can be obtained. Then ordering $a = \tau_1\tau_2$, $b = \tau_1 + \tau_2$, $d = R_1\tau_2 + R_2\tau_1 + R_0(\tau_1 + \tau_2)$, other parameters can be obtained, the Eq. (2-13) can be obtained from the Eq. (2-12).

$$\begin{cases} R_1 = (\tau_1 c + \tau_2 R_0 - d)/(\tau 1 - \tau 2) \\ R_2 = c - R_1 - R_0 \\ C_1 = \tau_1/R_1 \\ C_2 = \tau_2/R_2 \end{cases} \tag{2-13}$$

2.3. Genetic marginalized particle filter algorithm

Traditional particle filters (PF) algorithm usually cannot obtain a linear state estimation from the measurement equation, and it has problems of large calculation quantity and particles lacking when estimating the non-linear state. So a novel genetic marginalized particle filter (GMPF) method for state of charge and state of energy estimation adaptive to multi-temperature conditions of lithium-ion batteries is proposed in this article: the genetic algorithm is used to improve the heavy sampling process of traditional particle filtering, to obtain higher calculation accuracy by increasing the complexity of smaller calculation, and the problem of particles lacking will be solved by this way; at the same time, according to the Rao-Blackwell theory in statistical science, the marginalization of part of the linear state variables during the calculation of particle filtering, the distribution of the post-test is similar to a single Gaussian distribution, the Karman filter is updated to improve the accuracy of prediction when the condition of the remaining non-linear state variables.

The basic idea of PF algorithm is to use the Monte Carlo method to generate a large number of random particles to approach the state of the post-testing state to achieve the state estimate, in the process of the PF's prediction and update, it only updates part of the particles, status estimation is obtained through weighted and obtained, it does not need to calculate the post-verification collaborative difference in the status. This method can be used in non-linear, non-Gauss distribution. Monte Carlo Thought is to use a large number of random samples in the state space to approach the post-test probability distribution function of the variable that is approximately required, compared with other filtering methods such as the KF algorithm, the EKF algorithm, and the UKF algorithm, the PF algorithm does not need to make any prior assumptions on the system state, in theory, it can be used for any random system described by a state space model. But the PF algorithm has the following two problems:

1. Particles degradation: In actual calculation, after several particles dissemination, only a few particles have a large value, the weight of the remaining particles is ignored, the post-test probability distribution of the system state cannot be effectively expressed by the particles set. As a result, the filtering performance decreases or even diverges.
2. Particles lacking: Although the problem of particles degradation can be avoided by resampling, a lot of particles will be copied from the same large power particles, it will reduce the particle type significantly, even in the end, there is only one particle with a value of 1, the PF algorithm will no longer be able to make the probability distribution correctly.

The steps of the GMPF algorithm are as follows. Firstly, a state space model of lithium-ion batteries is established based on the process model and observation model, the status variable of the lithium-ion batteries model is the SoC and SoE of the lithium-ion batteries, it is shown in the Eq. (2-14).

$$\begin{cases} x_{k+1} = f(x_k, i_k, w_k) = x_k - \dfrac{ni_k\Delta t}{\eta_i\eta_T\eta_n Q_n} + w_k \\ y_{k+1} = h(y_k, i_k, w_k) = k_0 - Ri_k - \dfrac{k_1}{x_k} - k_2 x_k + k_3 ln(x_k) + k_4 ln(1 - x_k) + v_k \end{cases} \tag{2-14}$$

In the Eq. (2-14), w_k is the process noise of the system, v_k is the system's observation noise, supposing $w_k \sim N(0, Q)$, $v_k \sim N(0, R)$, Δt is the sampling cycle, x_k is a state variable, $f(\bullet)$ is the state function, y_k is observation variable, $h(\bullet)$ is the observation function.

First of all, the algorithm needs to be initialized, n SoC initial particles $\{SoC_0^i\}_{i=1}^N$ and n SoE initial particles $\{SoE_0^i\}_{i=1}^N$ are generated according to the probability of first check, the weight of the particles is shown in the Eq. (2-15).

$$\{q_0^i\}_{i=1}^N = \frac{1}{N} \tag{2-15}$$

Particles status is updated, according to the system update equation, the prior probability samples $\{SoC_k^i\}_{i=1}^N$ and $\{SoE_k^i\}_{i=1}^N$ at the next moment are obtained. After the system obtains new observations, a new particles set $\{x_{0,i}\}^+$ is generated through the equation of state, then the predicted value of the observed value is obtained through the observation equation. The particle weight equation is shown in Eq. (2-16).

$$\begin{cases} \omega_k^i = \omega_{k-1}^i p\left(U_{L(k)} \mid SoC_k^i\right) = \omega_{k-1}^i p\left(U_{L(k)} - h\left(SoC_k^i\right)\right), i = 1, 2 \ldots, N \\ \psi_k^i = \psi_{k-1}^i p\left(U_{L(k)} \mid SoE_k^i\right) = \psi_{k-1}^i p\left(U_{L(k)} - h\left(SoE_k^i\right)\right), i = 1, 2 \ldots, N \end{cases} \tag{2-16}$$

In the Eq. (2-16), the error between the observed value and the predicted value of each particle is calculated, and then the weight of particles is obtained through the error. After that, normalizing the weight of the sampled particles, as shown in the Eq. (2-17).

$$\begin{cases} \omega_i^* = 1 \Big/ \sum_1^N \omega_i \\ \psi_i^* = 1 \Big/ \sum_1^N \psi_i \end{cases} \tag{2-17}$$

In the Eq. (2-17), the weight of the sampled particles is normalized to reduce the load of calculation, and the least mean square estimate needs to be calculated, the equation of least mean square estimation is shown in the Eq. (2-18).

$$\begin{cases} \widehat{SoC_k} \approx \sum_{i=1}^N \omega_k^i SoC_k^i \\ \widehat{SoE_k} \approx \sum_{i=1}^N \psi_k^i SoE_k^i \end{cases} \tag{2-18}$$

Using the new random sample distribution generated in the previous steps to calculate the effective particle number $N_{eff} = \frac{1}{\sum_{i=1}^N \left(\omega_k^i\right)^2}$. If the number of effective particles is less than the threshold of the set number of effective particles, through resampling (extracting particles with high weight and eliminating particles with low weight), a new particle set is generated, after resampling, the weight of each particle in the new particle set is $1/N$. Then the estimated value is output, $\bar{x}_k$ is the SoC estimation value and $\bar{z}_k$ is the SoE estimated value, they are shown in the Eq. (2-19).

$$\begin{cases} \bar{x}_k = \sum_{i=1}^N \omega_k(i) x_k(i) \\ \bar{z}_k = \sum_{i=1}^N \psi_k(i) x_k(i) \end{cases} \tag{2-19}$$

The idea of biological evolution in genetic algorithm is introduced into particle filter, genetic algorithm optimizes the particles set in the process of resampling. Due to the unique optimization ability of genetic algorithm, the efficiency of particles is optimized, and many particles with different weights are added, it effectively suppresses the weight degradation of particles and the dilution of samples. The optimization process is as follows.

Step 1: Sampling M particles from the initial distribution of the population, they are recorded as $x^i, i = 1, 2, 3 \ldots, n$.

Step 2: According to the state transition equation of particles, the particles time of k are updated.

Step 3: Based on the measurement equation, calculate the weight of each particle in the particle set at time of k.

Step 4: The fitness of each particle in the particle set is determined by the weight coefficient, and then genetic operations such as selection, crossover and mutation of genetic algorithm are carried out, taking into account the selection of a variety of high weight particles and the diversity of particles, a new particle set is iterated.

Step 5: Calculating the state estimation and variance estimation at time of k:

$$\begin{cases} x_k = \sum_{i=1}^n \omega_i x_k^2 \\ p_k = \sum_{i=1}^M \omega_k^i \left(x_k^i - \widehat{x}_k^i\right)\left(x_k^i - \widehat{x}_k^i\right)^T \end{cases} \tag{2-20}$$

Step 6: Using the equation $f(\bullet)$ of state f to predict the particles at the next moment, it is recorded as $x_{k+1}^{(i)} = f\left(\widetilde{x}_k^{(i)}\right) + \omega_k, i = 1, 2, 3, \ldots, n$;

Step 7: Letting $k = k + 1$, turning to step 3 at the next measurement time.

The marginalized particle filter algorithm samples directly from the edge distribution of the state vector, using edge distribution function $P(x_{1:k}|Z_{1:k}, u_{1:k})$ to replace $P(x_k|Z_{1:k-1}, u_{1:k})$, the predicted probability density can be obtained from it, and the predicted probability density is shown in the Equation

$$P(x_k|Z_{1:k}) \infty P(z_k|x_k) \int P(x_k|x_{k-1}) \times P(x_{k-1}|Z_{1:k-1}) dx_{k-1} \tag{2-21}$$

Because the integral result cannot be obtained directly, $P(x_{k-1}|Z_{1:k-1})$ can be estimated from the particle set at time of $k-1$. Therefore, $P(x_k|Z_{1:k-1})$ can be approximated by $\sum_{i=1}^{N} \omega_{k-1}^{i} P(x_k|x_{k-1}^{i})$. For the convenience of calculation, $q(x_k|Z_{1:k})$ can take the form similar to $q(x_k|Z_{1:k})$, it is shown in the Eq. (2-22).

$$\sum_{i=1}^{N} \omega_{k-1}^{i} q(x_k|Z_k, x_{k-1}^{i}) \tag{2-22}$$

The marginalized particle filter algorithm samples directly from the edge distribution function, it can reduce the variance of particle importance weight and increase the estimated value of effective sampling. The algorithm flow chart is shown in Fig. 2-2.

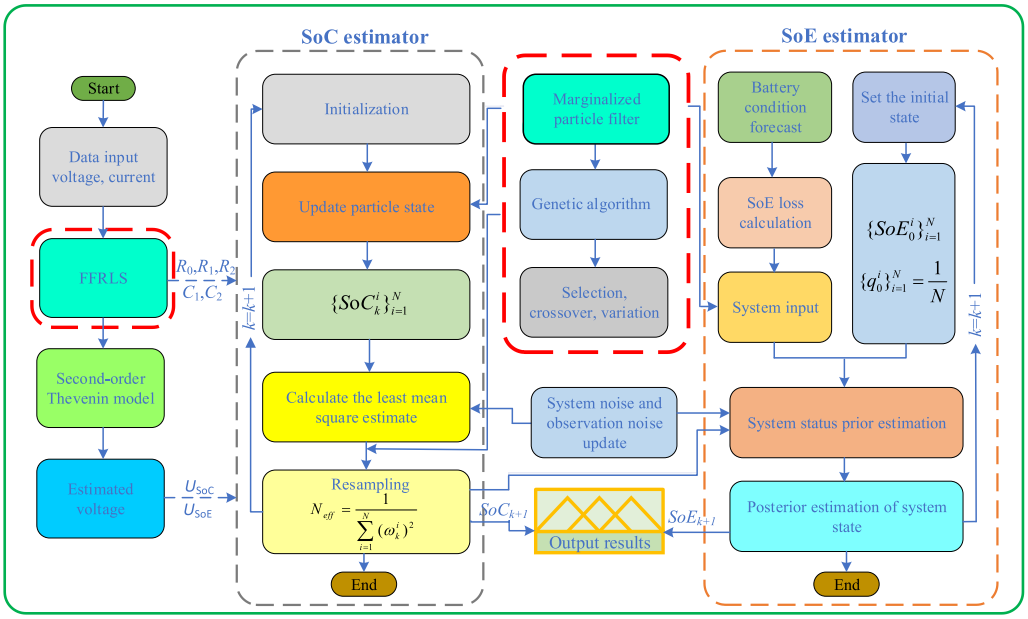

Fig. 2-2. The flow chart of genetic marginalized particle filter **a**lgorithm.

3. Experimental analysis

3.1. Results of parameter identification

The FFRLS algorithm is used to identify the parameters in the second-order Thevenin model under HPPC conditions and BBDST conditions with 15 °C, 25 °C, and 35 °C, respectively, and the discharge current is 1C under conditions of 15 °C and 25 °C, another discharge current is 0.5C under conditions of 35 °C. The results of parameter identification as shown in Fig. 3-1.

Each parameter in the second-order Thevenin model changes in real-time, the value of the same parameter is different under different working conditions, and the value of the same parameter is different at different temperatures. It can be seen from Fig. 3-1(g) that the error of online parameter identification is controlled within 5.61 %. It can be seen from Fig. 3-1(h) and (i) that the open circuit voltage decreases with the decrease of SoC/SoE, and the downward trend is similar at different temperatures, however, the open circuit voltage is different at different temperatures.

3.2. HPPC working condition verification

To verify the estimation accuracy of the GMPF algorithm for the joint estimation of SoC and SoE, for the same ternary lithium-ion battery, the test experiment of power lithium-ion battery is carried out at 15 °C, 25 °C, and 35 °C under HPPC working conditions. The rated capacity of the battery is 72 Ah, the battery charging and discharging equipment is BTS200-100-104 battery detection equipment, and the thermostat is SETH-Z-040L. The experimental platform is as shown in Fig. 3-2.

The specific steps of the HPPC working condition test are as follows: Step 1: First, conduct standard discharge on the battery, with the discharge current of 1C. After that, place it for 2 h, and then charge the battery with constant current and voltage until the SoC is 100 %. The charging current is set as 1C (72 Ah), the charging voltage is set as 4.2 V, and the cut-off condition is set as 2.5 A; Step 2: Leave the battery for 12 h to activate it, measure and record the voltage values at both ends of the battery. The voltage value at this time is the terminal voltage value when SoC = 1; Step 3: Leave the battery for 12 h to activate it, measure and record the voltage values at both ends of the battery. The voltage value at this time is the terminal voltage value when SoC = 1.3. Conduct current pulse test on lithium battery. First discharge the battery at 1C current for 10s, then let it stand for 40s, and then charge it at 1C current for 10s. The purpose is to return the battery to the SoC value before discharge and complete a set of experiments. The above pulse experiments all take time as the cut-off condition. (The discharge current is 1C at 15 °C and 25 °C, and 0.5C at 35 °C); Step 4: Then start discharging with a current of 1C. After discharging for 6 min (90 % SoC remains in the battery), let it stand for another 1 h. The cut-off condition is set to voltage 2.75 V. Finally, record the terminal voltage as the open circuit voltage U_{OC} at this time; Step 5: Repeat step 3 and step 4, discharge 10 % of the capacity in each cycle, record the relevant data at the SoC of 0.9, 0.8, 0.7…, 0.1, and provide data for the following parameter identification.

The sampling time of the experiment is 0.1 s. In order to restore the battery to the electrochemical balance and thermal balance state, the battery needs to be put aside for a long time between adjacent pulse tests. The whole experiment is mainly composed of a single repeated charge discharge pulse test. Calibration capacity is 65.76 Ah at 15 °C, 66.32 Ah at 25 °C, and 71.62 Ah at 35 °C. The estimation results of SoC and SoE joint estimation under different algorithms are compared through experimental data, and the GMPF algorithm is verified and analyzed through the comparison results. The experimental results as shown in Fig. 3-3.

In the verification experiment, the theoretical value of battery SoC is calculated by the AH algorithm, according to the definition of SoE, the theoretical value of SoE is calculated by power integration. The estimation results of the three algorithms are compared with the theoretical values respectively, and the estimation error is integrated and analyzed, it can be seen from Fig. 3-3, in the process of estimate of SoC and SoE, the tracking effect of the MPF algorithm is better than the PF algorithm, and the tracking effect of the GMPF algorithm is better than MPF algorithm, and the GMPF algorithm has the most stable estimation effect and the smallest error fluctuation. When the initial value of the algorithm is arbitrarily set to 0.8, the GMPF algorithm can converge at the beginning. Comparison of SoC and SoE estimation results in MAE and RMSE under HPPC condition as shown in Fig. 3-4.

It can see from Fig. 3-4, in the process of estimate SoC and SoE based on the GMPF algorithm, the SoC estimation under different temperature conditions, the average MAE of SoC estimation is 1.09 %, the average RMSE of SoC estimation is 1.09 %; the SoE estimation under different temperature conditions, the average MAE of SoE estimation is 0.81 %, the average RMSE of SoE estimation is 0.99 %. Through the error comparison under different conditions, it can be seen that GMPF algorithm has good robustness and excellent overall estimation performance, it has a very good estimation effect in the joint estimation of SoC and SoE of lithium-ion batteries. At the same time, it can be seen that PF is greatly affected by temperature, while GMPF algorithm is less affected by temperature. It can be seen that there is no strict linear relationship between the estimation accuracy of the algorithm and the ambient temperature, so the MAE value and RMSE of the algorithm do not strictly follow the increasing trend of temperature, but at the same temperature, it is obvious that the estimation error of GMPF algorithm is the smallest.

3.3. BBDST working condition verification

To further verify the estimation effect of the GMPF algorithm, verification experiments are carried out under more complex Beijing bus dynamic stress test (BBDST) conditions, and the temperatures are also set at 15 °C, 25 °C, and 35 °C respectively, and the improved GMPF algorithm is compared to analyze the advantages and disadvantages. The working condition parameters and description of BBDST are shown in Table 3-1.

BBDST working condition is obtained by collecting real data from Beijing buses. In the above table, Ph (KW) is the battery output power under real bus starting, accelerating, and taxiing conditions. In the experiment, the Pc (W) column data in the above table are used for constant power charge discharge experiment, and the data of Cumulative (s) is listed as the duration of a single step, the working condition column is the current status of the simulated bus. One cycle includes 19 single steps, and the duration of 1 cycle is 300 s. The experiment is carried out until the battery is discharged to the cut-off voltage. The experimental results as shown in Fig. 3-5.

It can be seen from Fig. 3-5 that SoC and SoE are estimated under BBDST working condition, the GMPF algorithm still maintains very good estimation ability and strong robustness. According to the experimental verification results, the three methods can effectively estimate the SoC and SoE of lithium batteries, however, both the MPF algorithm and the PF algorithm have large fluctuations and large errors in estimation, the improved GMPF algorithm has the best estimation effect. Although MPF can approximate the posterior distribution to a single Gaussian distribution, it can reduce the error of PF algorithm in the joint estimation of SoC and SoE to a certain extent. However, it cannot solve the problem of particle dilution, resulting in large estimation error. When the initial value of the algorithm is arbitrarily set to 0.8, the GMPF algorithm can converge at the beginning. Comparison of SoC and SoE estimation results in MAE and RMSE under BBDST condition as shown in Fig. 3-6.

It can see from Fig. 3-6, in the process of estimate SoC and SoE based on the GMPF algorithm, the SoC estimation under different temperature conditions, the average MAE of SoC estimation is 0.95 %, the average RMSE of SoC estimation is 0.98 %; the SoE estimation under different temperature conditions, the average MAE of SoE estimation is 1.15 %, the average RMSE of SoE estimation is 1.21 %. The experimental results show that the GMPF algorithm can well realize the joint estimation of SoC and SoE of power lithium-ion battery.

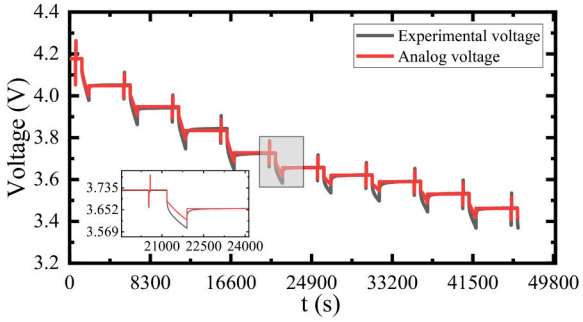

(a) The voltage under HPPC conditions of 15℃

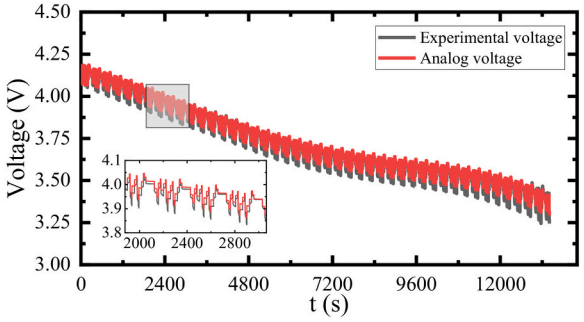

(b) The voltage under BBDST conditions of 15℃

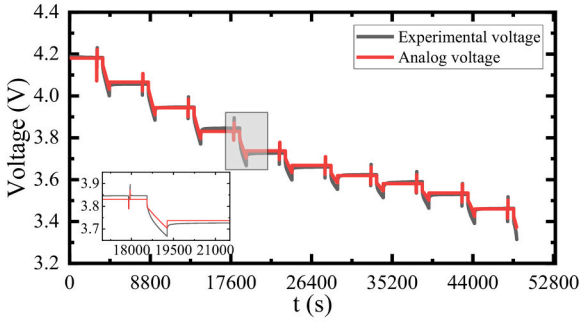

(c) The voltage under HPPC conditions of 25℃

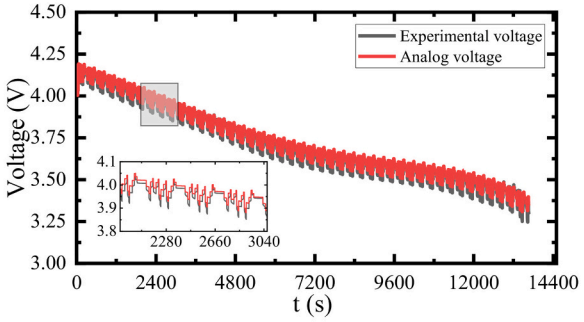

(d) The voltage under BBDST conditions of 25℃

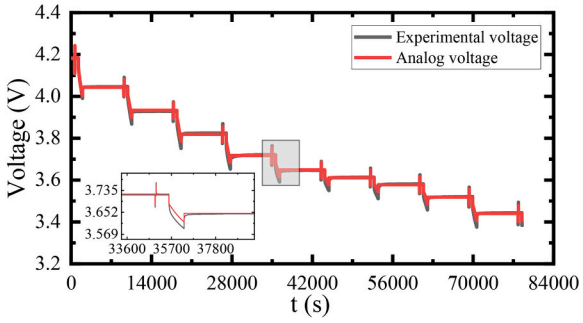

(e) The voltage under HPPC conditions of 35℃

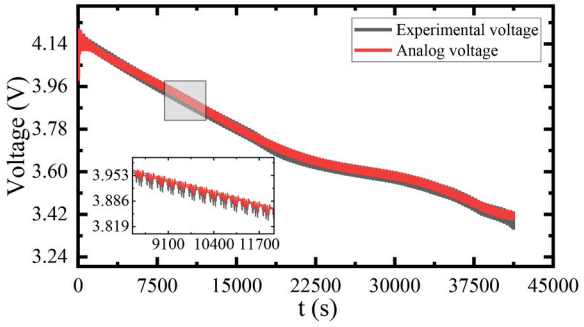

(f) The voltage under BBDST conditions of 35℃

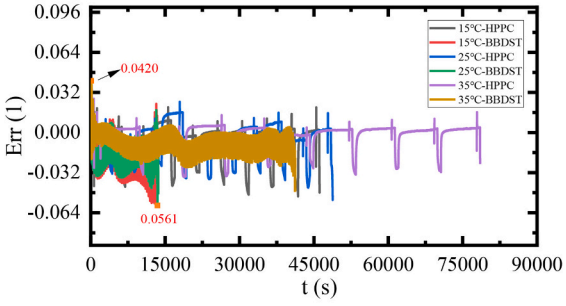

(g) The error of parameter identification at different temperatures

Fig. 3-1. The results of parameter identification.

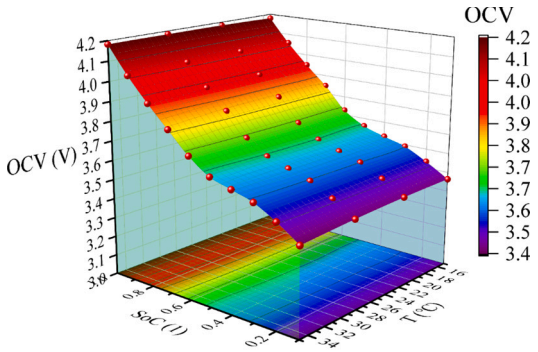

(h) The relationship between open circuit voltage and SoC at different temperatures

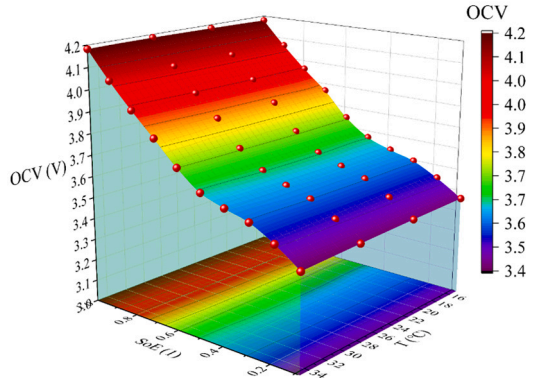

(i) The relationship between open circuit voltage and SoE at different temperatures

Fig. 3-1. (*continued*).

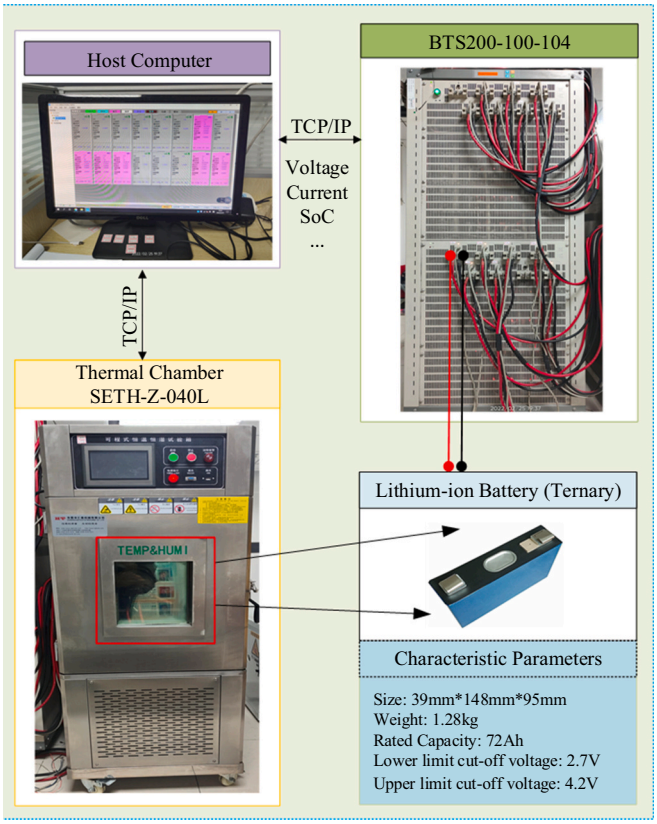

Fig. 3-2. The experimental platform.

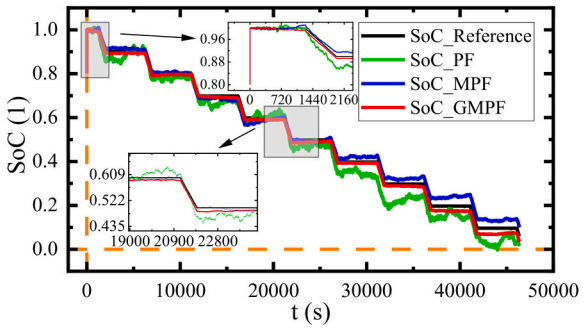

(a) SoC estimation results at 15℃

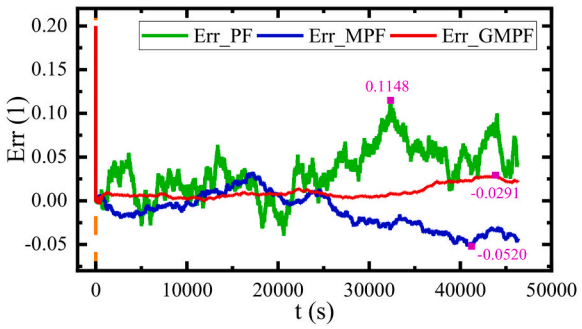

(b) SoC estimation error at 15℃

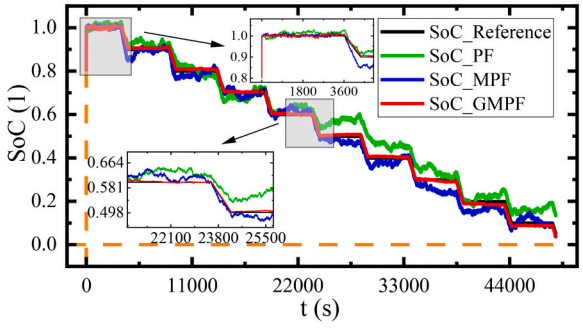

(c) SoC estimation results at 25℃

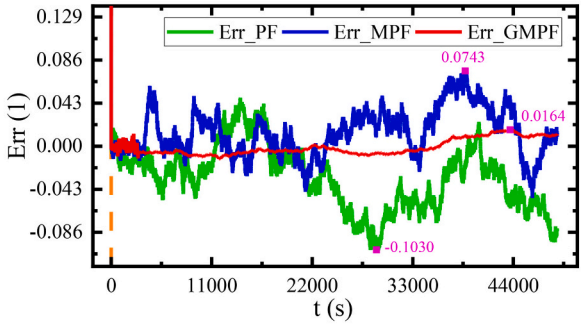

(d) SoC estimation error at 25℃

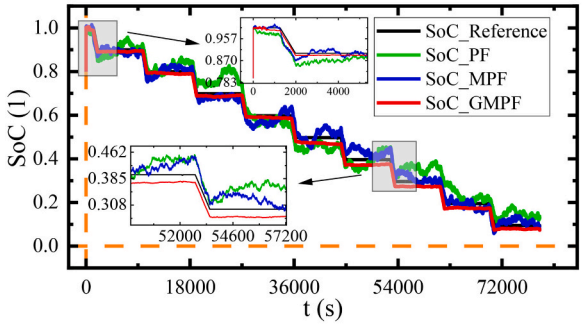

(e) SoC estimation results at 35℃

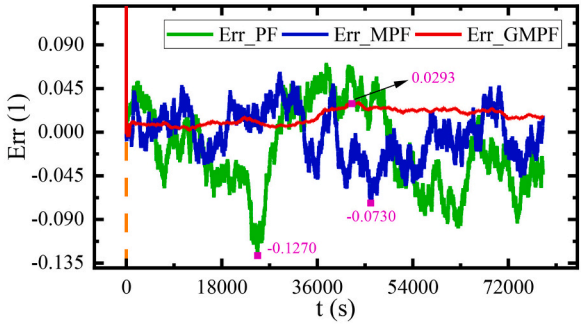

(f) SoC estimation error at 35℃

Fig. 3-3. The experimental results under HPPC conditions.

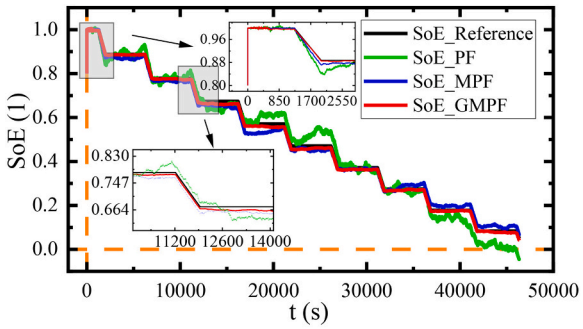

(g) SoE estimation results at 15℃

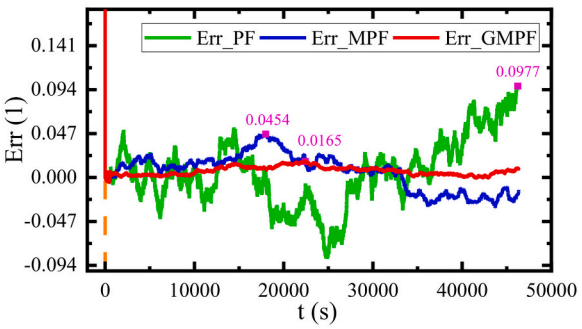

(h) SoE estimation error at 15℃

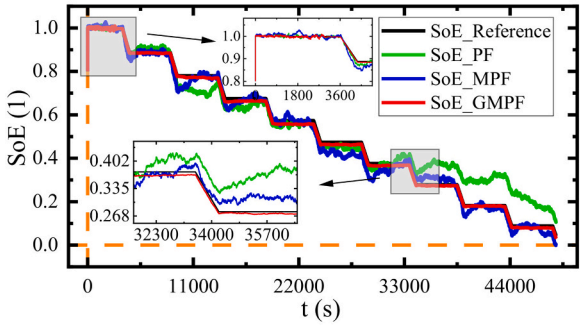

(i) SoE estimation results at 25℃

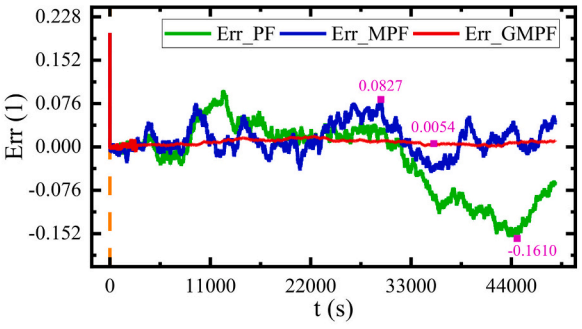

(j) SoE estimation error at 25℃

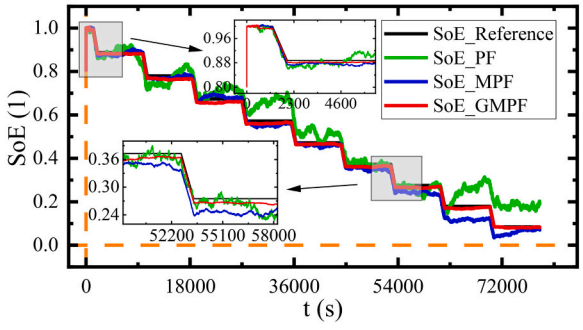

(k) SoE estimation results at 35℃

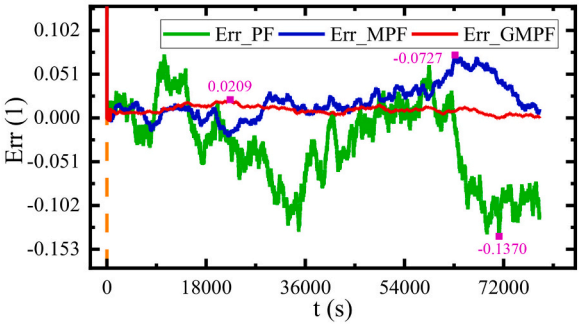

(l) SoE estimation error at 35℃

Fig. 3-3. (*continued*).

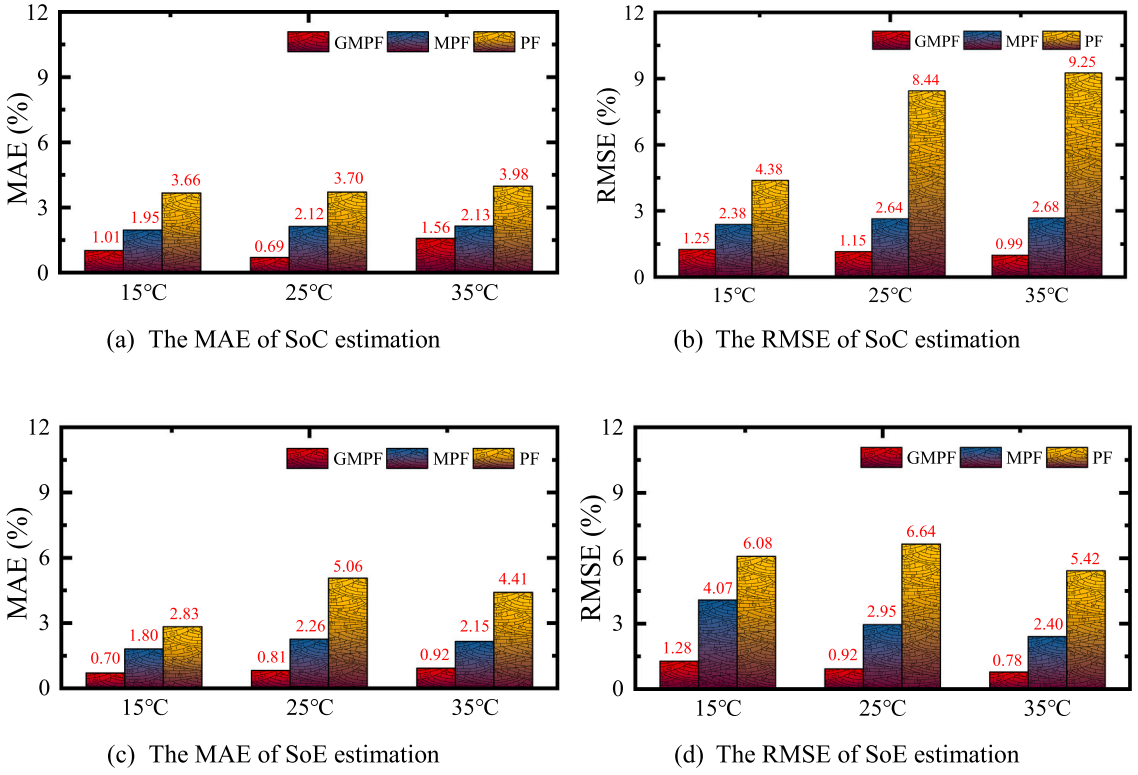

(a) The MAE of SoC estimation

(b) The RMSE of SoC estimation

(c) The MAE of SoE estimation

(d) The RMSE of SoE estimation

Fig. 3-4. Comparison of SoC and SoE estimation results in MAE and RMSE under HPPC condition.

Table 3-1
BBDST working condition parameters and description.

Ph (KW)	Pc (W)	Single-step (s)	Cumulative (s)	Working condition
37.5	69	21	21	Start
72.5	135	12	33	Accelerate
4.5	9	16	49	Glide
−15.0	−27	6	55	Braking
37.5	69	21	76	Accelerate
4.5	9	16	92	Glide
−15.0	−27	6	98	Braking
72.5	135	9	107	Accelerate
92.5	174	6	113	Rapid acceleration
37.5	69	21	134	Accelerate
4.5	9	16	150	Glide
−15.0	−27	6	156	Braking
72.5	135	9	165	Accelerate
92.5	174	6	171	Rapid acceleration
37.5	69	21	192	Accelerate
4.5	9	16	208	Glide
−35.0	−66	9	217	Braking
−15.0	−27	12	229	Braking
4.5	9	71	300	Parking

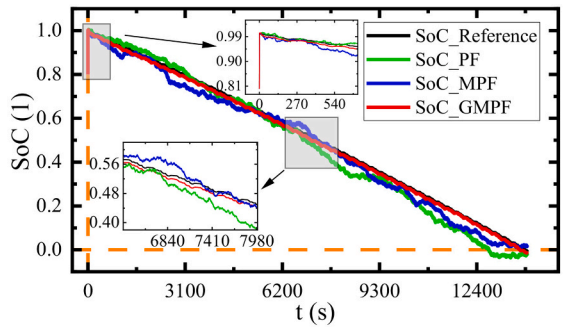

(a) SoC estimation results at 15℃

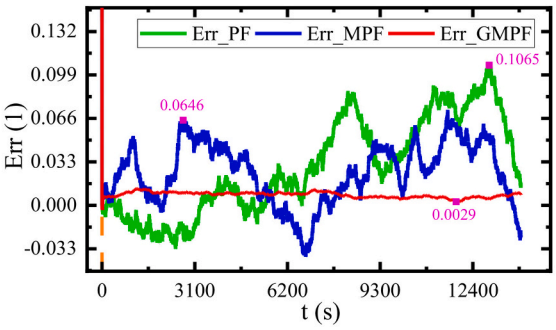

(b) SoC estimation error at 15℃

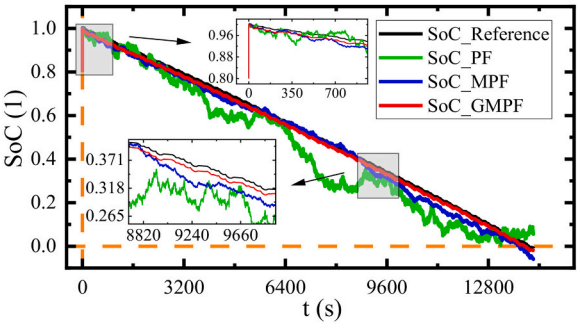

(c) SoC estimation results at 25℃

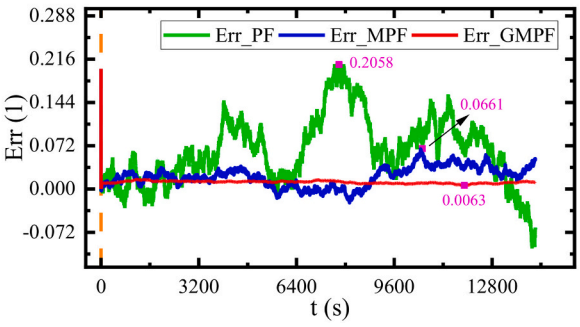

(d) SoC estimation error at 25℃

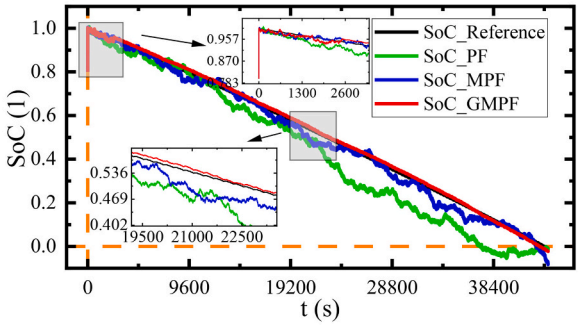

(e) SoC estimation results at 35℃

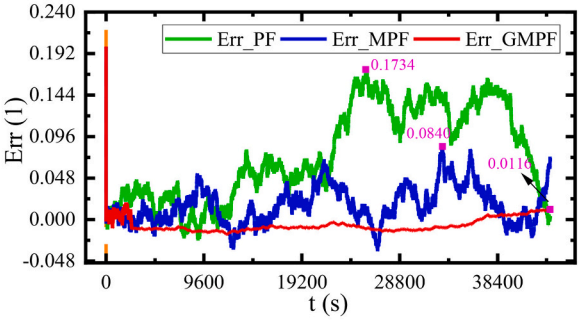

(f) SoC estimation error at 35℃

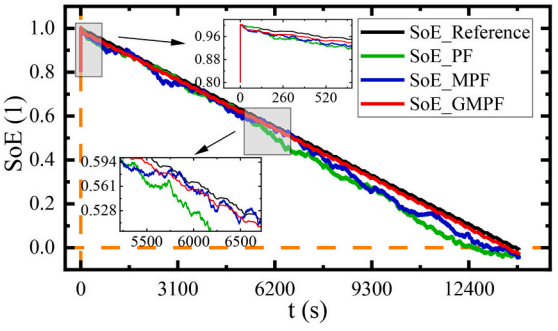

(g) SoE estimation results at 15℃

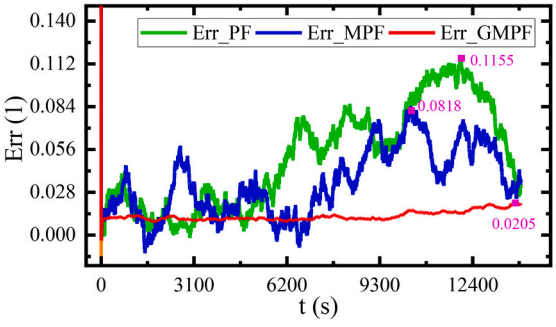

(h) SoE estimation error at 15℃

Fig. 3-5. The experimental results under BBDST conditions.

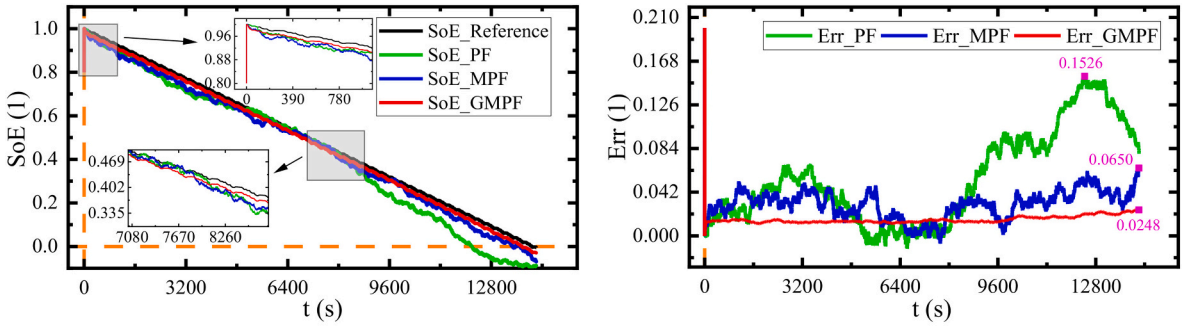

(i) SoE estimation results at 25℃ (j) SoE estimation error at 25℃

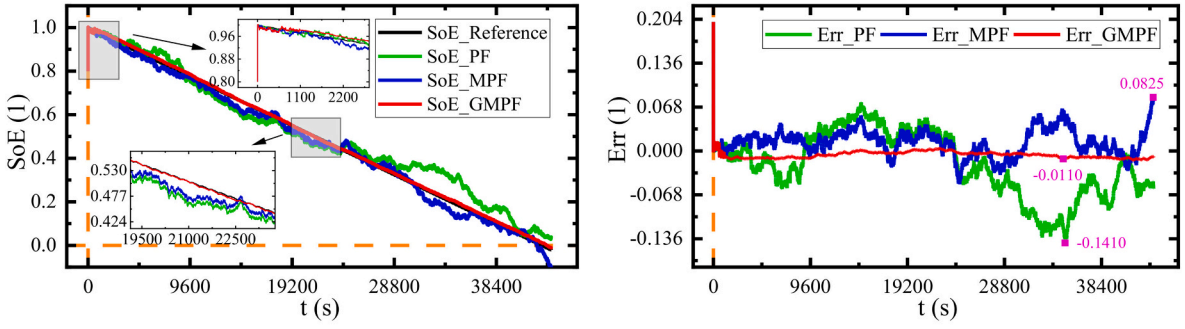

(k) SoE estimation results at 35℃ (l) SoE estimation error at 35℃

Fig. 3-5. (*continued*).

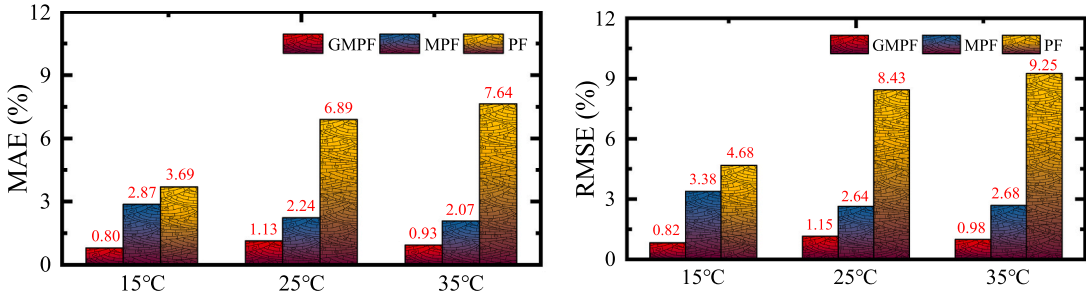

(a) The MAE of SoC estimation (b) The RMSE of SoC estimation

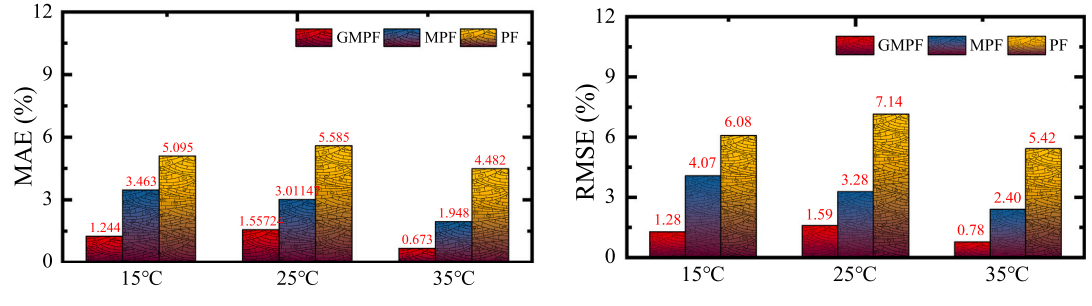

(c) The MAE of SoE estimation (d) The RMSE of SoE estimation

Fig. 3-6. Comparison of SoC and SoE estimation results in MAE and RMSE under BBDST condition.

4. Conclusions

SoC and SoE of the lithium-ion battery have always been the focus and difficulty of BMS system condition monitoring, to achieve a high-precision collaborative estimation of SoC and SoE, based on the second-order RC equivalent circuit model, this paper realizes the online identification of model parameters through the FFRLS algorithm. It solves the problem that offline parameter identification data processing is not timely and cannot be characterized in real-time. For the traditional PF algorithm, this paper proposes the following improvements: the genetic algorithm is used to improve the re-sampling process of the traditional PF algorithm, which will solve the problem of particles lacking in the traditional PF algorithm; according to the Rao-Blackwell theory in statistical science, the marginalization of part of the linear state variables during the calculation of particle filtering, the distribution of the post-test is similar to a single Gaussian distribution, the Karman filter is updated to improve the accuracy of prediction when the condition of the remaining non-linear state variables.

The improved GMPF algorithm is used to jointly estimate the SoC and SoE of lithium-ion batteries, it is verified under various working conditions and ambient temperatures: Under the HPPC working condition of 15 °C to 35 °C, the estimation accuracy of SoC is improved by 77.90 % on average, the estimation accuracy of SoE is improved by 81.94 % on average; under the BBDST condition of 15 °C to 35 °C, the estimation accuracy of SoC is increased by 84.86 % on average, the estimation accuracy of SoE is improved by 78.8 % on average. The feasibility of the GMPF algorithm for the joint estimation of SoC and SoE of lithium-ion batteries is verified, compared with the traditional PF algorithm, the GMPF algorithm has higher estimation accuracy and stronger robustness.

The scheme proposed in this paper has at least two obvious advantages: first, it can reduce the bad mutual coupling effect of SoC and SoE values, estimate SoC and SoE simultaneously at the same time scale, and improve the estimation accuracy of SoC and SoE; Secondly, it can be applied to a variety of working environment temperatures, and can obtain high estimation accuracy in a variety of working environment temperatures.

The GMPF algorithm can provide an effective reference for BMS system development and upgrading, but it also has shortcomings. For example, the ambient temperature range considered in this paper is not enough, and the working conditions of lithium-ion batteries in extremely low temperature, extremely high temperature, temperature over time, high and low voltage, and other harsh environments are not considered, and the experimental object of this paper is the battery cell, without considering the situation of the battery pack, so in the follow-up study, we will make further analysis for the above situation.

CRediT authorship contribution statement

Xianyi Jia: Conceptualization, Methodology, Software, Investiga-tion, Formal analysis, Writing – original draft, Validation. **Shunli Wang:** Data curation, Writing – review & editing. **Wen Cao:** Visualization, Investigation. **Jialu Qiao:** Supervision. **Xiao Yang:** Resources, Valida-tion. **Yang Li:** Resources. **Carlos Fernandez:** Resources.

Declaration of competing interest

No conflict of interest exists in the submission of this manuscript, and the manuscript is approved by all authors for publication.

Data availability

The data that support the findings of this study are available from the corresponding author upon reasonable request.

Acknowledgments

The work is supported by the National Natural Science Foundation of China (Nos. 62173281, 61801407), Sichuan Science and Technology Program (Nos. 23ZDYF0734, 23NSFSC4444), Dazhou City School Cooperation Project (No. DZXQHZ006), Technopole Talent Summit Project (No. KJCRCFH08), and Robert Gorden University.

References

[1] M.K. Baek, B.D. Shin, Hybrid operation strategy for demand response resources and energy storage system, J. Electr. Eng. Technol. 17 (1) (2022) 25–37.
[2] Y. Wen, et al., Progress in polymer separators for lithium-ion batteries, Polym. Mater. Sci. Eng. 37 (1) (2021) 292–299.
[3] Y.P. Wu, et al., Strategies for rational design of high-power lithium-ion batteries, Energy Environ. Mater. 4 (1) (2021) 19–45.
[4] N.S. Mubenga, T.A. Stuart, IEEE, A bilevel equalizer for lithium ion batteries, in: IEEE National Aerospace and Electronics Conference (NAECON), 2018, pp. 3–16. Dayton, OH.
[5] I. Jarraya, et al., An online state of charge estimation for lithium-ion and supercapacitor in hybrid electric drive vehicle, J. Energy Storage 26 (2019) 36–54.
[6] L. Zhou, et al., State estimation models of lithium-ion batteries for battery management system: status, challenges, and future trends, Batteries-Basel 9 (2) (2023) 78–101.
[7] K. Laadjal, A.J.M. Cardoso, Estimation of lithium-ion batteries state-condition in electric vehicle applications: issues and state of the art, Electronics 10 (13) (2021) 5–28.
[8] G. Zhang, et al., Study on the suppression effect of cryogenic cooling on thermal runaway of ternary lithium-ion batteries, Fire-Switzerland 5 (6) (2022) 124–136.
[9] C. Yang, et al., An advanced strategy of ?metallurgy before sorting? for recycling spent entire ternary lithium-ion batteries, J. Clean. Prod. 361 (2022) 66–90.
[10] J.H. Meng, et al., Overview of lithium-ion battery modeling methods for state-of- charge estimation in electrical vehicles, Appl. Sci. Basel 8 (5) (2018) 69–96.
[11] Z.M. Xi, et al., Accurate and reliable state of charge estimation of lithium ion batteries using time-delayed recurrent neural networks through the identification of overexcited neurons, Appl. Energy 305 (2022) 15–37.
[12] Y.J. Chen, et al., Remaining available energy prediction for lithium-ion batteries considering electrothermal effect and energy conversion efficiency, J. Energy Storage 40 (2021) 55–69.
[13] S.L. Wang, et al., An improved coulomb counting method based on dual open- circuit voltage and real-time evaluation of battery dischargeable capacity considering temperature and battery aging, Int. J. Energy Res. 45 (12) (2021) 17609–17621.
[14] Z.H. Cui, et al., A comprehensive review on the state of charge estimation for lithium-ion battery based on neural network, Int. J. Energy Res. 46 (5) (2022) 5423–5440.
[15] X.Q. Ren, et al., A method for state-of-charge estimation of lithium-ion batteries based on PSO-LSTM, Energy 234 (2021) 1225–1237.
[16] Y.W. Zhang, et al., Estimation of state of charge integrating spatial and temporal characteristics with transfer learning optimization, Meas. Sci. Technol. 34 (4) (2023) 258–276.
[17] L.L. Gong, et al., Voltage-stress-based state of charge estimation of pouch lithium- ion batteries using a long short-term memory network, J. Energy Storage 55 (2022) 2621–2638.
[18] X. Yang, et al., A novel fuzzy adaptive cubature Kalman filtering method for the state of charge and state of energy co-estimation of lithium-ion batteries, Electrochim. Acta 415 (2022) 59–81.
[19] X. Lai, et al., A joint state-of-health and state-of-energy estimation method for lithium-ion batteries through combining the forgetting factor recursive least squares and unscented Kalman filter, Measurement 205 (2022) 889–893.
[20] X. Lai, et al., A novel method for state of energy estimation of lithium-ion batteries using particle filter and extended Kalman filter, J. Energy Storage 43 (2021) 9–25.
[21] S.Z. Zhang, X.W. Zhang, A novel low-complexity state-of-energy estimation method for series-connected lithium-ion battery pack based on “representative cell” selection and operating mode division, J. Power Sources 518 (2022) 26–40.
[22] S.Z. Zhang, X.W. Zhang, A novel non-experiment-based reconstruction method for the relationship between open-circuit-voltage and state-of-charge/state-of-energy of lithium-ion battery, Electrochim. Acta 403 (2022) 66–80.
[23] K. Laadjal, A.J.M. Cardoso, A review of supercapacitors modeling, SoH, and SoE estimation methods: issues and challenges, Int. J. Energy Res. 45 (13) (2021) 18424–18440.
[24] F.L. An, et al., A novel state-of-energy simplified estimation method for lithium-ion battery pack based on prediction and representative cells, J. Energy Storage 63 (2023) 2115–2137.
[25] P. Shrivastava, et al., Comprehensive co-estimation of lithium-ion battery state of charge, state of energy, state of power, maximum available capacity, and maximum available energy, J. Energy Storage 56 (2022) 66–80.
[26] J.H. Zhao, et al., Review of state estimation and remaining useful life prediction methods for lithium-ion batteries, Sustainability 15 (6) (2023) 56–72.
[27] Yang, Y., et al., Recent progresses in state estimation of lithium-ion battery energy storage systems: a review. Trans. Inst. Meas. Control.: p. 2–19.
[28] M. Wei, et al., State of charge estimation for lithium-ion batteries using dynamic neural network based on sine cosine algorithm, Proc. Inst. Mech. Eng. Part D-J. Automob. Eng. 236 (2–3) (2022) 241–252.
[29] T.E. Fan, et al., Simultaneously estimating two battery states by combining a long short-term memory network with an adaptive unscented Kalman filter, J. Energy Storage 50 (2022) 456–470.
[30] Y.J. Wang, et al., Probability based remaining capacity estimation using data- driven and neural network model, J. Power Sources 315 (2016) 199–208.
[31] Zhang, S.Z., N. Peng, and X.W. Zhang, An application-oriented multistate estimation framework of lithium-ion battery used in electric vehicles. Int. J. Energy Res.: p. 11–26.
[32] L. Ma, C. Hu, F. Cheng, State of charge and state of energy estimation for lithium- ion batteries based on a long short-term memory neural network, J. Energy Storage 37 (2021) 26–37.
[33] X. Wei, et al., Unscented particle filter based state of energy estimation for LiFePO4 Batteries using an online updated model, Int. J. Automot. Technol. 23 (2) (2022) 503–510.